The slowdown of growth rate controls the single-cell distribution of biofilm matrix production via a SinI-SinR-SlrR network

Zhuo Chen[a], Brenda Zarazúa-Osorio[b], Priyanka Srivastava[b, d], Masaya Fujita[b]*, and Oleg A. Igoshin[a,c]*

[a] Systems, Synthetic and Physical Biology Program, Rice University, 6100 Main St., Houston, TX 77005, USA,

[b]Department of Biology and Biochemistry, University of Houston, 3455 Cullen Blvd., Houston, TX, 77204, USA

[c]Department of Bioengineering, Center for Theoretical Biological Physics, Department of Chemistry, and Department of Biosciences, Rice University, 6100 Main St., Houston, TX 77005, USA

[d] Present address: Priyanka Srivastava, Department of Pathology Microbiology and Immunology, Vanderbilt University Medical Center, Nashville, Tennessee, USA.

Abstract

In *Bacillus subtilis*, a master regulator Spo0A controls several cell-differentiation pathways. Under moderate starvation, phosphorylated Spo0A (Spo0A~P) induces biofilm formation by indirectly activating genes controlling matrix production in a subpopulation of cells via a SinI-SinR-SlrR network. Under severe starvation, Spo0A~P induces sporulation by directly and indirectly regulating sporulation gene expression. However, what determines the heterogeneity of individual cell fates is not fully understood. In particular, it is still unclear why, despite being controlled by a single master regulator, biofilm matrix production and sporulation are mutually exclusive on a single-cell level. In this work, with mathematical modeling, we showed that the fluctuations in the growth rate and the intrinsic noise amplified by the bistability in the SinI-SinR-SlrR network could explain the single-cell distribution of matrix production. Moreover, we predicted an incoherent feed-forward loop: the decrease in the cellular growth rate activates matrix production by increasing in Spo0A phosphorylation level but represses it via changing the relative concentrations of SinR and SlrR. Experimental data provide evidence to support model predictions. In particular, we demonstrate how the degree to which matrix production and sporulation appear mutually exclusive is affected by genetic perturbations.

Importance:

The mechanisms of cell-fate decisions are fundamental to our understanding of multicellular organisms and bacterial communities. However, even for the best-studied model systems we still lack a complete picture of how phenotypic heterogeneity of genetically identical cells is controlled. Here, using *B. subtilis* as a model system, we employ a combination of mathematical modeling and experiments to explain the population-level dynamics and single-cell level heterogeneity of biofilm gene expression. The results demonstrate how the two cell fates, biofilm matrix production and sporulation, can appear mutually exclusive without explicitly inhibiting one another. Such a mechanism could be used in a wide range of other biological systems.

Introduction

To adapt to various environmental conditions, bacterial cells can differentiate into different cell types (1). *B. subtilis* is one of the best-understood model systems for studying bacterial cell differentiation. Upon starvation, a subpopulation of *B. subtilis* cells can differentiate into matrix producers, which form long chains and express and secret extracellular biofilm matrix (2, 3). As a result, given the right environmental conditions, cells encase themselves in the extracellular matrix and thereby form a biofilm (4). At later stages of starvation, *B. subtilis* cells can further activate another cell differentiation pathway and transition into spores (5). Notably, in biofilms different cell types co-exist, forming a highly heterogeneous community (6, 7).

Both the matrix production and sporulation are activated by the same transcriptional master regulator, Spo0A. Upon starvation, Spo0A is phosphorylated to become an active form as a transcription factor (Spo0A~P) through multicomponent phosphorelay composed of five kinases on the top, and two intermediate phosphotransferases (8, 9). Among five kinases, KinA and KinC play major roles to control sporulation and biofilm formation, respectively (10-12). The cellular concentration of Spo0A~P gradually increases in a pulsatile manner over the course of starvation, leading to up-/down-regulation of genes and operons having binding sites (named 0A-box) for the phosphoproteins (10, 13-15). However, many of the 0A boxes deviate from the consensus sequence (5′-TGTCGAA-3′) (13). Thus, the binding affinity of Spo0A~P to the 0A-box changes with the variation of the consensus sequence (10). At early times of starvation, the relatively low concentrations of Spo0A~P preferentially bind to the high-affinity 0A-boxes in the genes and operons involved in biofilm formation. When starvation persists, the high dose of Spo0A~P occupies the weak-affinity sites in the genes and operons involved in sporulation (10, 16).

While genes involved in sporulation are directly controlled by Spo0A~P, biofilm formation is controlled via an additional SinI-SinR-SlrR network, which is also under the control of Spo0A~P, leading to the expression of a set of genes and operons, including the *tapA* (formerly named *yqxM*)-*sipW*-*tasA* operon (Fig. 1A)(17, 18). At the top of the regulatory network, Spo0A~P activates the expression of *sinI* (19). Downstream of *sinI*, *sinR* is constitutively and independently transcribed (20). The activity of SinR, a master regulator of biofilm formation is regulated by two antagonists, SinI and SlrR, that can form alternative complexes with SinR, respectively, preventing the formation of $SinR_4$ (the active tetramer form of SinR). On the one hand, SinI dimer ($SinI_2$) interacts with SinR dimer ($SinR_2$) and forms SinI-SinR heterodimer ($SinI_2{\cdot}SinR_2$). On the other hand, SlrR dimer ($SlrR_2$) associates with $SinR_2$ and forms $SlrR_2{\cdot}SinR_2$ heterotetramer (21-23). The expression of *slrR* is also repressed by $SinR_4$, thereby resulting in a double-negative feedback loop between SinR and SlrR. This double-negative feedback loop between SinR and SlrR forms a bistable switch and controls matrix production and cell chaining (24, 25). In this SinI-SinR-SlrR network, Spo0A~P concentration serves as the input by directly controlling SinI expression. Therefore, the Spo0A and SinI-SinR-SlrR network systems precisely control the level of SinR during growth and starvation conditions. During growth under nutrient-rich conditions, little if any Spo0A~P is present, and thus the Spo0A-controlled SinI, an antagonist of SinR transcription factor, is not expressed highly. As a result, the constitutively expressed SinR represses a set of genes and operons involved in biofilm formation, including the *tapA* operon, allowing cells to grow (26). Upon starvation, relatively low concentrations of Spo0A~P generated via the phosphorelay activate the expression of SinI (27), which in turn sequesters and thereby antagonizes SinR (17, 18). SinR is also sequestered by forming a $SlrR_2{\cdot}SinR_2$ heterotetramer during this period(21). When starvation persists, cellular concentrations

of Spo0A~P further increase with the decrease in cell growth rate and directly stimulate the expression of genes involved in sporulation (13, 16, 28).

Intriguingly, despite being both activated by Spo0A~P, sporulation and matrix production are mutually exclusive: the matrix production drops significantly in cells initiating sporulation (24, 29). As a result, the population-average biofilm matrix production level decreases at the late stages of starvation (24). These observations are attributed to the repression of SinI expression by high Spo0A~P levels and to the effect of sporulation initiation on the gene dosage of *sinR* and *slrR* (24). However, our recent results showed that artificially induced high Spo0A~P levels cannot repress the expression of matrix production genes, which questions the explanation that high Spo0A~P levels and sporulation repress matrix production (11). Therefore, the mechanisms of mutually exclusive cell fates and of the decrease of biofilm matrix production at late stages of starvation are still not fully understood.

Understanding cell fate decision in the biofilm matrix production is only possible on the level of individual *B. subtilis* cells since the expression of biofilm matrix genes is highly heterogeneous (30, 31). Our recent work showed that this heterogeneity is controlled through the effects of two different kinases, leading to proper matrix production (11). In particular, we showed that KinC reduces single-cell heterogeneity of Spo0A~P resultant from the noise in cellular growth rate and thereby increases the fraction of cells that activate matrix production (11). However, the results also suggest that noise in growth rate is not sufficient to fully explain the single-cell distribution of matrix-production gene expression (11).

In this work, using stochastic modeling, we investigate how the extrinsic noise in growth rate and intrinsic noise in the SinI-SinR-SlrR network affect the distribution of matrix-producing cells at different times post starvation. Furthermore, we use our models to uncover the competing effects of the slowdown of growth rate on the SinI-SinR-SlrR network. This model is used to explain the dynamics of biofilm matrix production under different genetic perturbations and to investigate why biofilm matrix production and sporulation appear mutually exclusive on a single-cell level. Experimental tests of the model predictions confirm the proposed mechanisms of cell-fate control.

Results

An increase in Spo0A~P is necessary but not sufficient for matrix-production

Previously, assuming a deterministic relationship between Spo0A~P levels and *tapA* expression, we failed to quantitatively match the single-cell distribution of matrix production (11). In particular, the model predicted that a fraction of matrix-producing cells is higher than the experimentally observed fraction (11). Since the fluctuations in the SinI-SinR-SlrR network are known to affect matrix production (25, 30), we hypothesized that stochastic properties of the SinI-SinR-SlrR network that controls the relationship between Spo0A~P levels and *tapA* expression could reduce the fraction of matrix-producing cells. To test this hypothesis, we constructed a detailed mathematical model of this network and used it to examine the relationship between Spo0A~P levels and TapA reporter concentration in deterministic and stochastic simulations.

The schematics of the modeled network shown in Fig. 1A include transcriptional and post-translational interactions between SinI, SinR, and SlrR (see Materials and Methods for details). However, the significance of the double-negative feedback loop between SinR and SlrR on matrix production is unclear. To answer this question, we first investigated how the steady-state concentration of TapA is affected by the Spo0A~P level via the SinI-SinR-SlrR network. As Fig. 1B shows, our model with the

deterministic simulations demonstrated that, when Spo0A~P level is low, the system has only one stable steady state (Fig. 1B, blue solid line) in which *tapA* expression is not activated and TapA concentration is low. When Spo0A~P level is higher than a threshold, a matrix-production-on steady state appears (Fig. 1B, red solid line) and the system shows bistability. If we further increase Spo0A~P concentration (> 0.4 μM), the steady-state value of TapA would not change much (Fig. 1B, red solid line). This can be explained that the expression of SinI only requires a low threshold of Spo0A~P (10); when Spo0A~P goes higher, the expression of SinI would be saturated and cannot be further increased. Thus, the activation of Spo0A~P is necessary but not sufficient for matrix production: when Spo0A~P level is lower than the threshold, the *tapA* cannot be activated; when Spo0A~P level is higher than the threshold, both the high and the low *tapA* expression states are present. In the latter regime, the expression is hysteretic in our deterministic simulations, *i.e.,* cells starting with a high level of *tapA* expression remain high, whereas cells starting with a low level will remain low.

To test the possibility of switching between steady states, we constructed a stochastic version of the network (see Methods for details) and conducted a stochastic simulation of the model for fixed low (0.05 μM) and high (1μM) Spo0A~P levels, *i.e.,* in the monostable and bistable conditions for the deterministic model. As Fig. 1C shows, for high Spo0A~P concentration, the *tapA* expression could be activated in a stochastic manner (red line); whereas, for low Spo0A~P concentration, the *tapA* expression remains around the low level (blue line). The results demonstrated that fluctuations of the SinI-SinR-SlrR network can lead to stochastic activation of *tapA* expression but only if Spo0A~P is sufficiently high. In other words, high Spo0A~P is necessary but not sufficient for *tapA* expression.

Extrinsic noise in growth rate and intrinsic noise in the SinI-SinR-SlrR network can explain the individual-cell distribution of matrix expression

Spo0A~P levels increase with the slowdown of cell growth rate during nutrient starvation (15, 28, 32, 33). Thus, next, we investigated whether the combination of the intrinsic noise in the SinI-SinR-SlrR network and the fluctuations of growth rate can explain the single-cell level heterogeneity of *tapA* expression. To reproduce the single-cell level distribution of *tapA* expression in a starving community, following our previous work (11), we used a Moser-type model (34) to describe the dynamics of the population-average growth rate (Fig. 2A, solid line). We also assumed that the cell generation time follows a normal distribution with a coefficient of variation, CV=0.25. The shaded area in Fig. 2A shows the range of the growth rate in ~70% of cells ($\pm\sigma$). It was shown that the distribution of single-cell Spo0A~P concentrations could be sufficiently explained by the fluctuations in the growth rate (15). Thus, we assumed that the Spo0A~P level is determined by the growth rate, so the noise in the Spo0A~P level fully originates from the growth rate fluctuations. Using the same model in our previous work (11), we predicted how the Spo0A~P levels changes with the growth rate in the wild-type (WT) strain and the strain harboring the deletion of *kinA* (Δ*kinA*) and *kinC* (Δ*kinC*) that were shown to affect *tapA* expression dynamics. (Fig. 2B). Based on the dynamics and fluctuation of the growth rate, we modeled the dynamics and distribution of Spo0A~P levels in different strains (Fig. 2C). Furthermore, to investigate the single-cell level heterogeneity of *tapA* expression, we performed stochastic simulations of the SinI-SinR-SlrR network for different cell lineages in parallel (see Supplemental Methods for details). To this end, Spo0A~P levels were used as the input and were sampled from the predicted distribution. Then, we calculated the distribution of *tapA* expression levels at different times (after 4, 6, 8, and 12 hours of culture, denoted as T4, T6, T8, and T12) in each of the three strains (WT, Δ*kinA*, and Δ*kinC*). As Fig. 2D shows, the model predicts that the majority of cells have very low *tapA* expression (the first bin of the

histogram in 2D). Moreover, the frequency of the first bin is lower in the WT than in the Δ*kinC* and Δ*kinA* strains and is decreasing with time. These results were consistent with the experimental data from our previous work (Fig. S1).

Therefore, the results shown in Fig. 2 revealed the mechanisms in which the noise in growth rate and the SinI-SinR-SlrR network affect the heterogeneity of *tapA* expression. Our model predicts that the intrinsic noise of the SinI-SinR-SlrR network ensures that the activation of Spo0A is a permissive but not instructive signal for matrix production. Under starvation conditions, the average cellular growth rate decreases with time (Fig. 2A). As a result, cellular Spo0A~P levels increase with time (15), so the fraction of cells not expressing *tapA* decreases with time (Fig. 2D, WT, T4-T8, note the change in the y-axis scale in each panel). In the Δ*kinA* strain, Spo0A~P level is lower than in the WT strain (Fig. 2C, after T5), so the probability of expressing *tapA* is also lower in the Δ*kinC* strain than in the WT strain (Fig. 2D, WT vs. Δ*kinA*, note the change in y-axis scale in each panel). Moreover, we found that the *tapA* expression level at T12 is lower than that at T8 (Fig. 2D, Δ*kinA*, note the change in the y-axis scale in each panel). These results were consistent with published experimental results (24).

In the Δ*kinC* strain, Spo0A~P level was lower than in the other two at early times T4 (Fig. 2C), so the probability of expressing *tapA* was also lower in the Δ*kinC* strain than in the other two (Fig. 2D, note the change in y-axis scale in each panel). At later times (after T6), the average Spo0A~P level became higher in the Δ*kinC* strain than in the other two (Fig. 2C), but individual cells of the Δ*kinC* strain do not significantly express the *tapA* at later times as compared with the other two strains (Fig. 2D, T6-T12, note the change in y-axis scale in each panel). Our simulation showed that the single-cell distribution of *tapA* expression is not in a steady state: when we fixed the growth condition at T6 and ran the simulation for a longer time, the fraction of *tapA*-expressing cells would increase further (Fig. S5). Moreover, our previous work showed that KinC reduces single-cell heterogeneity of Spo0A~P in the fast-growing cells and thereby increases the fraction of cells that activate *tapA* expression (11). For fast-growing cells in the population, KinC still acts as a source of phosphoryl groups, so the deletion of *kinC* (Δ*kinC*) results in lower probabilities of expressing *tapA* due to lower levels of Spo0A~P than in the WT strain. As a result, the fraction of cells expressing *tapA* would be lower in the Δ*kinC* strain than in the WT strain at every time point (Fig. 2D, Δ*kinC*). Thus, these results suggest that, in single cells, the effect of KinC on *tapA* expression depends on the growth rate.

Slowdown of cellular growth has two opposing effects on the SinI-SinR-SlrR network

Notably, our model shows the decrease of *tapA* expression at T12 for all the strains considered (Fig. 2D, T12). For wild-type cells, this result is consistent with previous experimental observations (24). We, therefore, set to understand the mechanisms of the decrease in *tapA* expression at late times in our model. A previous study suggests that the observed decrease of *tapA* expression under prolonged starvation is associated with (i) the decreased levels of SinI due to the direct repression of *sinI* by high levels of Spo0A~P, and (ii) increased levels of SinR over SlrR due to changes in gene dosage during sporulation (24). Both mechanisms result in the increased active SinR ($SinR_4$ tetramer), leading to the repression of *tapA* expression. However, in our model, neither the repression of SinI expression by high Spo0A~P levels nor the sporulation process was explicitly included. Instead, gene dosages and protein concentrations change as a function of cellular growth rate. This indicates the slowdown of the growth rate can somehow negatively regulate *tapA* expression via the SinI-SinR-SlrR network.

In our model, growth rate mainly affected cellular protein concentrations by affecting their dilution rate. For stable proteins like SinR, the effective degradation rate (the sum of the degradation rate and

dilution rate caused by growth) is dominated by the dilution rate, and the slowdown of growth will lead to increases in their concentrations. In contrast, SlrR is known to be quickly degraded *in vivo* (35), so the change in growth rate has a relatively small effect on the effective degradation rate (Fig. 3A). In addition, our model suggested that the SinR/SlrR ratio is controlled by the gene dosage effect related to the position of the genes on chromosomal DNA (24) as was the case for KinA and Spo0F (14, 15, 32). In general, gene distance from the origin of chromosome replication (*oriC*) influences gene copy number in a periodical manner during the growth cycle of a bacterial cell (36). During DNA replication (C-period) (Fig. S2A), genes proximal to *oriC* (ori) are replicated first and will have a higher gene dosage relative to the genes proximal to the replication terminus (*ter*) (Fig. 2BC). After replication is complete, the gene dosage returns to a 1:1 ratio. A slowdown of growth has a greater effect on the cell cycle period than on the C-period and thereby increases the duration of the period during which there is no active DNA replication, resulting in a 1:1 gene dosage (Fig. S2). Therefore, cells growing slower are expected on average to have less excess in gene dosage for ori-proximal genes. In the case of the SinI-SinR-SlrR network, *slrR* is located at the origin proximal region while *sinI* and *sinR* genes are at the origin distal region. Thus, when cells grow rapidly, the dosage of *slrR* exceeds those of *sinI* and *sinR* for a longer part of a cell cycle leading to a higher *slrR* production rate. However, when the growth rate slows down, cell-cycle-averaged excess gene dosage for *slrR* is smaller than when the growth rate is fast; the relative production rate of *sinR* to *slrR* gene increases with growth slowdown. In summary, different protein degradation rates and different gene positions cause the ratio of SinR and SlrR to increase with decreasing growth rate (Fig. 3A).

To understand the impact of this effect in our model, we first use a deterministic model of the SinI-SinR-SlrR network and compute a bifurcation diagram in response to independently changing Spo0A~P concentration and the growth rate (Fig. 3B). The result indicates that bistability (and existence *tapA* expression state) requires Spo0A~P level to be higher than a threshold (as we saw in 1B) and the growth rate to be not too slow (shaded region in Fig. 3B). If we fixed Spo0A~P at a relatively high level (Fig. 3B, dashed line), the system is bistable but only at high growth rates (Fig. 3C). As growth slows down, there will be an insufficient amount of SinI and SlrR to fully inhibit the activity of SinR (Fig. 3A). As a result, the system would enter the monostable region and the matrix-production-on state (Fig. 3C, red solid line) would disappear, *i.e., tapA* will be repressed. Stochastic simulation under fixed growth rates and Spo0A~P levels confirmed that bistability only exists when both the Spo0A~P level and the growth rate are high enough (Fig. S3).

In light of these results, we propose that the growth rate affects *tapA* via two opposing mechanisms acting on the SinI-SinR-SlrR network (Fig. 3D). On the one hand, by regulating the upstream phosphorelay network, the slowdown of growth rate raises Spo0A~P level via increasing KinA level P (15) and thereby activates SinI expression (27). This would lead to sequestration of SinR into the SinI·SinR complex and lead to derepression of *tapA*. On the other hand, the slowdown of growth directly increases the relative concentration of SinR to SlrR, decreasing the amount of SinR sequestered in the $SlrR_2 \cdot SinR_2$ complex. This effect leads to an increase in the free and active $SinR_4$ form, resulting in the repression of *tapA*. In other words, there is an incoherent feed-forward loop between the growth slowdown and *tapA* expression, and this motif is known to produce non-monotonic dynamics of gene expression (37, 38).

Note that experimentally Spo0A~P concentration and the growth rate are not independent and a slowdown of growth results in the increase of Spo0A~P (15). Explicitly testing the above incoherent feed-forward hypothesis, therefore, requires genetic perturbations data that affect the Spo0A~P

concentration, *e.g*., those affecting phosphorelay and perturbations affecting growth dynamics (i.e. how cell growth rate changes with time).

Slowdown of growth rate directs the decrease of *tapA* expression at late stages of growth

To validate the above-proposed model that the slowdown of growth rate is the main reason for the decrease of *tapA* expression at late times, we predicted the dynamics of *tapA* expression levels under different genetic perturbations that change the dynamics of Spo0A~P levels. To this end, in addition to the WT and the strains harboring the deletion of two phosphorelay kinases (Δ*kinA* and Δ*kinC*) considered in Fig. 2, we also investigated the effects of Sda, an inhibitor of KinA by forming an inactive complex Sda-KinA (39). Deletion of *sda* (Δ*sda*) is expected to raise Spo0A~P levels as a result of increased KinA activity, leading to promoted sporulation (39, 40), whereas deletion of *kinA* (Δ*kinA*) will do the opposite since it is the major sporulation kinase (9, 12). Regarding KinC, our previous data suggest that KinC decreases Spo0A~P levels by removing a phosphoryl group from Spo0A~P at relatively early stages of sporulation, and thus deletion of *kinC* (Δ*kinC*) promotes increasing Spo0A~P levels and sporulation frequencies (11). Therefore, investigating these strains may allow us to separate the effects of Spo0A~P concentration and the growth rate on matrix production.

Using a deterministic model of phosphorelay from our prior work (11, 14, 32), we determined Spo0A~P concentration as a function of the growth rate in each of the above strains. As Fig. 4A shows, for all of the strains Spo0A~P increased with a decrease in growth rate. As expected, Spo0A~P levels in the WT strain were higher than in those in the Δ*kinA* strain but lower than those in the Δ*sda* strain. In the Δ*kinC* strain, Spo0A~P levels were lower than in the WT strain under high growth rates at early times of culture. However, Spo0A~P levels became higher in the Δ*kinC* strain than in the WT strain under low growth rates at later times of culture. Superimposing these trajectories on the bifurcation diagram, one can note that all of these values left the bistable region at around the same value of growth rate, due to the bistability region boundary being nearly vertical (Fig. 4A, dashed line). Therefore, we expect that *tapA* expression would decline at around the same growth rate in all three strains despite distinct Spo0A~P dynamics can be seen in each of them. Assuming that growth-rate dynamics are the same for all strains (11), we can use the stochastic simulation of the model to predict *tapA* expression. The results predicted that in all of the strains, *tapA* expression decreased at about the same time (~10h, Fig. 4B). Alternatively, if the hypothesis that the high Spo0A~P levels leading to sporulation drive the decrease of *tapA* expression is correct (24), our simulations would expect very different times of the peaks of *tapA* expression in those strains (Fig. S4). Critically, in the Δ*kinA* strain, since the Spo0A~P level would not go beyond the sporulation threshold and thus the sporulation efficiency is very low (12), we predicted the decrease of *tapA* expression to happen later (Fig. S4).

To test the prediction that the decrease of *tapA* expression occurs simultaneously in all strains (WT and deletion mutants), we performed experimental measurements of *tapA* expression dynamics in those strains with *β*-gal reporter. In the results shown in Fig. 4C, the peak of *tapA* expression occurred at 8~10h in the tested strains except for the Δ*kinC* strain where the peak is slightly earlier (6-7 h). Notably and similarly to the other strains tested, the decrease in *tapA* expression after 9~10h was observed in the Δ*kinA* strain where little sporulation is triggered (Fig. 4C). These results support our hypothesis that the decrease of *tapA* expression is due to the slowdown of growth rate, rather than the high Spo0A~P levels or the sporulation. Thus, these data are qualitatively consistent with the idea that the incoherent feed-forward-loop mechanism through the SinI-SinR-SlrR network is important to control *tapA* expression.

Even though our model supports general trends in the observed *tapA* dynamics, the experimental results in the Δ*kinC* strain showed that the *tapA* expression peaked at around 6-7 h and then decreased earlier than in the other strains (Fig. 4C). These experimental data were slightly different from the modeling data (Fig. 4B). Moreover, the experimental data showed that, in the Δ*sda* stain, the *tapA* expression decreases much more rapidly (Fig. 4C) than predicted (Fig. 4B). These inconsistencies may be due to the early onset of sporulation in the Δ*kinC* and Δ*sda* strains (11). Spore formation may repress *tapA* expression and/or interfere with β-galactosidase activities. These effects were not considered in the model.

Perturbation to cell growth rate alters *tapA* expression dynamics

The results thus far indicated that perturbing the Spo0A~P dynamics does not significantly affect the time when *tapA* expression peaks. However, if our hypothesis that the slowdown of growth rate is the main reason for the decrease of *tapA* expression is correct, we expect that a change in growth dynamics would shift the time of *tapA*-expression peak. To demonstrate this with our model, we used alternative growth rate dynamics as inputs to our model (Fig. 5A). Stochastic simulation of the model predicted that, if the growth rate slows down more rapidly (Fig. 5A, red curve), the *tapA* expression would start to decrease earlier, and the resulting maximum *tapA* expression level would also be significantly lower than the unperturbed cell growth rate dynamics (Fig. 5B).

To test this prediction experimentally, we artificially changed cell growth rate by reducing nitrogen source (diluted glutamate by 10 times) in MSgg medium (Modified MSgg medium, See Materials and Methods). Under culture conditions in the modified MSgg medium, the nitrogen source would be depleted faster, and therefore cell growth would slow down earlier than in the original MSgg medium. As Fig. 5C shows, in the cells grown in the modified MSgg medium, the decrease of *tapA* expression happens much earlier, and the peak value becomes much lower, which is consistent with the model prediction (Fig. 5B). These results further support our hypothesis that the slowdown of growth is the primary reason for the decrease of *tapA* expression at the late stages of starvation.

Slowdown of cell growth leads to mutually exclusive cell fates

Since our model explains the population-level decrease of *tapA* expression at late times, we hypothesized that it can also explain why sporulation and biofilm matrix expression appear mutually exclusive on a single-cell level. To test this hypothesis, we predicted the *tapA* expression and sporulation levels in single cells of the WT, Δ*sda*, and Δ*kinC* strains, using stochastically varying but on average slowing cell growth dynamics (Fig. 2A) as an input. Following our previous study (16), cells displaying high-threshold Spo0A~P levels were considered sporulating. The fraction of *tapA*-expressing cells between sporulating (spo) and non-sporulating (non-spo) cells at T8 was then calculated by simulation (Fig. 6A). These results showed that, in the WT strain, about 28% (0.28) of non-sporulating (non-spo) cells activate *tapA* expression, but this fraction is only 9% (0.09) for sporulating cells (spo) (Fig. 6A). These results were qualitatively consistent with the published experimental results of Ref. (24), which indicates that our model can also explain single-cell distributions of matrix production and sporulation. Thus, our model predicts that mutual exclusiveness can be explained by the repression of matrix production at the slow growth rate at which WT cells initiate sporulation.

Furthermore, we can use our model to predict how genetic perturbation in phosphorelay affects mutual exclusiveness. Notably, our results indicated that the fraction of *tapA*-expressing cells increased more in the Δ*sda* strain relative to the WT strain (0.34 vs 0.25, Fig. 6A). However, when the increase in *tapA*-expressing cells in the Δ*sda* vs WT strains is broken down by sporulation status, we note that this

increase was larger in the sporulating cells (from 0.09 to 0.28) than in non-sporulating cells (from 0.21 to 0.36) (Fig. 6A). On the other hand, in the Δ*kinC* strain, the fraction of *tapA*-expressing cells was lower than in the WT strain (0.25 vs 0.15, Fig. 6A). This decrease in the fraction of *tapA*-expressing cells is only slightly lower in the sporulating cells (~33% from 0.09 to 0.06) than in non-sporulating cells (~39% from 0.28 to 0.17) (Fig. 6A). These simulation results predict that the deletion of *sda* (Δ*sda)* not only increases the overall fraction of *tapA*-expressing cells but also increases the fraction of the cells that both activate *tapA*-expressing and sporulation. On the other hand, the deletion of *kinC* (Δ*kinC*) decreases the fraction of *tapA*-expressing cells among sporulating cells, as well as all the cells. In other words, the deletion of *sda* (Δ*sda)* would "weaken" the mutual exclusiveness of matrix production and sporulation, while the deletion of *kinC* (Δ*kinC*) would only slightly affect it.

To verify these predictions, we experimentally measured *tapA* expression (with *PtapA*-GFP) and sporulation (with forespore-specific SpoIIQ expression using *PspoIIQ*-mCherry) in the WT, Δ*sda*, and Δ*kinC* strains at single-cell levels. We used a fluorescent reporter encoding a proteolytically unstable GFP-LCN to monitor *tapA* expression by minimizing the parameter of GFP stability (with *PtapA-gfp-LCN*) (24, 41). To determine which cells are sporulating, we counted cells expressing forespore-specific mCherry driven by the *spoIIQ* promoter since *spoIIQ* is only expressed during sporulation in the forespore (42) (see supplemental method for details). Fluorescent images of the cells cultured in MSgg were taken after 8 hours (Fig. 6B). Then, using a GFP threshold we calculated the fraction of *tapA*-expressing cells in sporulating and non-sporulating cells for each strain (Fig. 6C). Among all cells, the overall fraction of *tapA*-expressing cells in the WT strain (0.20) was lower than that in the Δ*sda* strain (0.27) but higher than that in the Δ*kinC* strain (0.11) (Fig. 6C). Moreover, in all of these strains, this fraction of *tapA*-expressing cells was higher in non-sporulating cells than in sporulating cells (Fig. 6C). However, when we compared the sporulating (spo) and non-sporulating (non-spo) cells, the fold-change in the fractions of *tapA*-expression cells was smaller in the Δ*sda* (non-spo/spo = 0.29/0.24 = 1.21) than in the Δ*kinC* (non-spo/spo = 0.13/0.07 = 1.86) and WT (non-spo/spo = 0.27/0.13 = 2.08) strains. These experimental results were qualitatively consistent with the model predictions (Fig. 6A).

To summarize, our results provide another way to explain the mutually exclusive cell fates between biofilm formation and sporulation. At later stages of starvation, a slowdown of growth rate leads to an increase in sporulation probability. Meanwhile, the probability of *tapA* expression would decrease due to the effect of slow growth on SinR/SlrR ratio, leading to increased SinR. As a result, the probability that a sporulating cell also activates *tapA* expression is low, so the sporulation and matrix production appear as mutually exclusive cell fates. In the Δ*sda* strain, due to higher Spo0A~P levels with increased KinA activity, the fraction of the *tapA*-expressing cells is higher than in the WT strain (Fig. 6). Moreover, in the Δ*sda* strain, the threshold of growth rate for sporulation is lower, and thus the sporulation happens earlier than in the WT strain. As a result, the increase of the fraction of *tapA*-expressing cells in the Δ*sda* strain is more significant in sporulating cells than in non-sporulating cells. As our previous work shows (11), in the Δ*kinC* strain, Spo0A~P levels are lower than in the WT strain at early times of starvation, so the fraction of the *tapA*-expressing cells is lower than in the WT strain (Fig. 6). Moreover, KinC acts as a sink of phosphoryl groups in the slow-growing cells in a culture population (11). As a result, sporulation happens earlier in the Δ*kinC* strain with increased levels of Spo0A~P at relatively early times of starvation. The acceleration of sporulation in the Δ*kinC* strain, therefore, is similar in the mechanism but weaker as compared to the Δ*sda* strain. As a result, the deletion of *kinC* (Δ*kinC*) only slightly "weakens" the mutual exclusiveness of matrix production and sporulation.

Discussion

In a community of *B. subtilis* cells, at the onset of starvation, a subset of cells activates matrix production, leading to biofilm formation. However, at later stages of starvation, cells stop producing matrix and initiate sporulation. The master regulator Spo0A and the SinI-SinR-SlrR network play a critical role in the regulation of biofilm matrix production (18, 25, 43). In this work, we showed that the cellular growth rate would affect matrix production via an incoherent feed-forward loop (Fig. 3D). On the one hand, the slowdown of growth rate activates matrix production via an increase of Spo0A~P level and induction of SinI. On the other hand, the slowdown of growth represses matrix production by affecting the dosage between SinR and SlrR.

At the early stages of starvation, the slowdown of growth rate leads to the increase of Spo0A~P concentration via its effect on KinA concentration and the DNA replication cycle (14, 32). Our previous work shows that the noise of growth rate would affect the distribution of Spo0A~P in a culture population and thereby affects the heterogeneity of *tapA* expressing cells in a culture population (11). Here, our model predicts that Spo0A~P is necessary for the expression of matrix genes, but it is not sufficient for the activation of matrix production (Fig. 2C). When Spo0A~P is low, the SinI-SinR-SlrR network only has a high-SinR-low-SlrR steady state, and *tapA* expression cannot be activated due to repression by SinR. When Spo0A~P increases, the SinI-SinR-SlrR network enters the bistable region (Fig. 2C), so the *tapA* expression could be activated by decreasing SinR level via the stochastic fluctuations in the SinI-SinR-SlrR network. The bistability of the SinI-SinR-SlrR network ensures that only a subset of cells can activate matrix production, reducing the cost of matrix production and saving resources as a bet-hedging strategy. The fluctuations in the SinI-SinR-SlrR network were known to be critical in determining the transition between the matrix-producing state and non-matrix-producing states (25, 30). Our model qualitatively reproduces the distribution of *tapA* expression in individual cells (Fig. 1D, Fig S1), indicating that the heterogeneity of matrix production in a starving community could be mostly explained by the noise in the growth rate and the fluctuations in the SinI-SinR-SlrR network.

At late stages of growth, Spo0A~P level would be saturated for activating SinI expression (27). The slowdown of growth rate at late stages mainly affects matrix production through the cellular concentration of SinR and SlrR (Fig. 3). Due to different gene locations of *sinR* and *slrR* and different protein stability of their gene products (Figs. 3A), changes in growth rate cause DNA-replication associated gene dosage effect (Fig. S2BC). As a result, when the growth rate slows down, the concentration of SinR increases faster than SlrR, and eventually, the free and active form of SinR represses *tapA* expression at late times (Fig. 3CD). Similar effects of growth rate can be found in other bacterial models of cellular regulatory networks (44-47).

Previously, it has been demonstrated that cells entering sporulation stop *tapA* expression (24). To explain this mutual relationship between sporulation and matrix production, two mechanisms have been proposed: first, high Spo0A~P levels negatively affect SinI expression and eventually repress matrix production, and second, the change in the gene dosage between SinR and SlrR during sporulation also represses matrix production (24). Following this explanation, we would expect that the *tapA* expression would start to decrease earlier in the Δ*sda* strain because the Spo0A~P level increases more rapidly and the sporulation starts earlier than in the WT strain (Fig. S3). On the other hand, in the Δ*kinA* strain, Spo0A~P level is too low to trigger sporulation; thus, we would expect that the *tapA* expression would start to decrease at later times in the Δ*kinA* strain than in the WT strain (Fig. S3). As Fig. 4 shows, however, our data shows that the *tapA* expression would start to decrease at about the same time in the

WT, Δ*kinA*, and Δ*sda* strains. Moreover, we showed that perturbing growth dynamics can change the time when *tapA* starts to decrease (Fig. 5). Our model also successfully explains why biofilm matrix production and sporulation are mutually exclusive, which is consistent with experimental results (Fig. 6). These results indicate that, rather than sporulation and asymmetric division as proposed in the previous study (24), the slowdown of growth rate, is a major control mechanism to change the dosage of SinR and SlrR, eventually leading to repression of *tapA* expression.

In summary, our results provide a system-level understanding of the role of growth rate in controlling biofilm matrix production. By controlling Spo0A~P level and the dosage of SinR and SlrR, the slowdown of growth rate regulates biofilm matrix production via an incoherent-feed-forward network. This proposed model explains the population-level dynamics and single-cell level heterogeneity of biofilm gene expression. Specifically, our study reveals that mutually exclusive cell fates between biofilm matrix production and sporulation can be generated by incoherent feed-forward regulatory networks. This network motif defines a signal-window (or a time-window for a time-dependent signal) during which matrix production is possible. Therefore, other cell fates that are activated by the same signal but with a threshold outside of this window, e.g., sporulation, will only occur in the cells that are not expressing matrix. In other words, the cell fates appear mutually exclusive without explicitly inhibiting one another. Such a mechanism can be advantageous for cell survival under unforeseen conditions as a bet-hedging strategy and could be applicable in a wide range of other biological systems.

Materials and Methods

Computational Modeling

The equations, reactions, and procedures used for mathematical modeling are in the Supporting Text S1. Parameters used for simulations are included in Tables S1 and S2. The code is available to download in Github: https://github.com/Igoshin-Group/SinI-SinR-SlrR-data.

Strains, plasmids, and oligo DNAs

The strains and plasmids used are listed in Table S3. Oligo DNAs used for plasmid constructions are listed in Table x. *B. subtilis* strains used in this work are isogenic derivatives of the undomesticated and competent DK1042 (48). DK1042 is a derivative of strain NCIB 3610 forming a biofilm matrix (49). All mutant strains of *B. subtilis* were constructed by transformation with either chromosomal DNA or plasmid DNA as described by Harwood and Cutting (50). The standard recombinant DNA techniques including plasmid DNA construction and isolation using *Escherichia coli* DH5α were performed as described by Sambrook and Russell (51). A plasmid **pMF523** (*amyE::PspoIIQ-mCherry spc*) was constructed by ligating the PCR fragment containing the *spoIIQ* promoter and the coding region of mCherry into pDG1730 (52). The *spoIIQ* promoter region was amplified by PCR with primers omf42 and omf43 using chromosomal DNA from *B. subtilis* PY79 as the template. The mCherry coding region was amplified by PCR with primers om87 and om88 using pDR201 (53) as the template. The two PCR products were recovered from the agarose gel and purified using the gel extraction kit (Qiagen). The purified *PspoIIQ* DNA fragment was digested with *Eco*RI and *Hin*dIII. The purified mCherry DNA fragment was digested with *Hin*dIII and *Bam*HI. The digested DNA fragments were purified by the PCR purification kit (Qiagen). The purified *spoIIQ* promoter and mCherry DNA fragments were mixed and ligated with pDG1730 digested with *Eco*RI and *Bam*HI. The resulting plasmid was integrated into the *amyE* locus of the *B. subtilis* chromosomal DNA by double-crossover homologous recombination. A plasmid **pMF1154** (*thrC::PtapA-gfp-lcn erm*) was constructed by ligating the PCR fragment containing the *tapA* promoter and the coding region of GFP-LCN into pDG1664 (52). The *tapA* promoter region

was prepared from pMF712 with *Eco*RI and *Hin*dIII digestion (12). The digested DNA fragment containing the *tapA* promoter was recovered from the agarose gel and purified using the gel extraction kit (Qiagen). The GFP coding region was amplified by PCR with primers omf316 and om528 using pMF719 (*thrC::PtapA-gfp erm*) as the template (11). The PCR product containing *gfp-lcn* was recovered from the agarose gel and purified using the gel extraction kit (Qiagen). The purified PCR product was digested with *Hin*dIII and *Bam*HI and purified by the PCR purification kit (Qiagen). The purified *tapA* promoter and *gfp-lcn* DNA fragments were mixed and ligated with pDG1664 digested with *Eco*RI and *Bam*HI. The resulting plasmid was integrated into the *thrC* locus of the *B. subtilis* chromosomal DNA by double-crossover homologous recombination.

Media and culture conditions

Lysogeny broth (LB) medium (51) was used for routine growth of *E. coli* and *B. subtilis*. MSgg (Minimal salts glycerol glutamate) medium was used for biofilm formation and sporulation of *B. subtilis* (2). For nitrogen-depleted MSgg medium, L-glutamate was 10-fold diluted (0.05% final concentration, relative to the original 0.5% final concentrations). Cells were cultured with shaking (150 rpm) overnight in LB (5 ml) at 28°C. The overnight culture was transferred to fresh LB (10 ml) to an OD600 of 0.05. The fresh culture was incubated at 37°C with shaking (150 rpm) to the mid-log phase (OD600 ≈ 0.5) to synchronize cell growth. Then, the fresh culture was transferred to MSgg (20 ml) to an OD600 of 0.05 and incubated in a culture flask at 37°C with shaking (150 rpm). Culture samples were collected at the indicated time points and assayed for a specific activity of β-galactosidase reporter or processed for microscopy. Cell growth in liquid media was measured using a spectrophotometer by reading the optical density at 600 nm (OD600). Strains harboring reporter genes at the non-essential *thrC* locus were supplemented with 1 mg ml^{-1} of L-threonine in the MSgg medium. When making solid agar media, 1.5% (w/v) agar was included. Antibiotics were used for the selection of transformants at the following concentrations: 10 μg ml^{-1} of tetracycline, 100 μg ml^{-1} of spectinomycin, 20 μg ml^{-1} of kanamycin, 5 μg ml^{-1} chloramphenicol, and 1 μg ml^{-1} of erythromycin.

β-Galactosidase assay

B. subtilis undomesticated strains were grown in a liquid medium as described in the above section of Media and culture conditions. Samples were collected at indicated time points and β-galactosidase assays were performed as described (11). The mean activities of at least three independent experiments are shown with standard deviations.

Microscopy analysis

Cells collected at the specified times were spotted on MSgg medium containing 1% (wt/vol) agarose (ISC Bioexpress, E-3119-500) in a Gene Frame chamber (Thermo Scientific, AB-0577; 65 mL, 1.5 by 1.6 cm) and covered by a cover glass. The cell samples were immediately examined using a fluorescence microscope (Olympus, model BX61) with an Olympus UPlanFL N 100X microscope objective. GFP and mCherry fluorescence were visualized using Chroma 41017 and Olympus U-MWG2 filter sets, respectively. Typical exposure times were 200 ms. The microscope system was operated using SlideBook image analysis software (Intelligent Imaging Innovations, Inc.) and the resulting images were processed as described (11). Representative images are shown. GFP and mCherry channels are shown in green and magenta pseudocolors, respectively. Using the same method as (11), we segmented the cells and calculated the pixel-wise mean fluorescence intensity of GFP and mCherry for each cell. For each image, the pixel-wise mean GFP/mCherry intensity of the no-cell area was calculated as background. The cells with *PtapA* activity significantly higher than the background were considered "*tapA*-

expressing cells", and the cells with *PspoIIQ* activity significantly higher than the background were considered "sporulating cells". Over 2000 cells were analyzed for each strain.

Supplemental Material

Figure S1: The experimentally observed distribution of *tapA* expression The distribution of mean-fluorescence intensity of *PtapA-GFP* in WT and Δ*kinC* cells at T4, T6, and T8. The value of the first bin was labeled on each histogram. Reproduced using data from Ref. (11).

Figure S2: Growth rate affects gene dosage for the replication-terminus proximal genes.
(A) The duration of the C period (replication) and the whole cell cycle as functions of growth rate.
(B and C) The change of the copy numbers of a replication-terminus proximal gene ($p = 1$) and a replication-origin proximal gene ($p = 0$) within a cell cycle. The copy numbers were plotted for growth rates equal to 0.6 h^{-1} (B) and 0.15 h^{-1} (C). For a gene proximal to the replication origin, the gene dosage is 2 during the whole cell cycle regardless of the growth rate. For a gene proximal to the replication terminus, the fraction of time that the gene dosage is equal to 2 is larger when the growth rate is lower.

Figure S3: The distribution of SlrR and SinR levels at different Spo0A~P levels and growth rates from stochastic simulations.

Figure S4: The traditional explanation of why *tapA* expression decreases at late times.
(A) The traditional model of how high Spo0A~P levels repress *tapA* expression. On the one hand, high Spo0A~P levels repress the expression of SinI. On the other hand, high Spo0A~P levels trigger sporulation, which changes the dosage between SinR and SlrR and eventually represses the expression of *tapA*.
(B) The Spo0A~P values as functions of growth rate in WT, Δ*kinA*, and Δ*sda* strains. The assumed threshold of Spo0A~P level that is sufficient to repress *tapA* expression is shown as the dashed line.
(C) The predicted dynamics of *tapA* expression with the traditional model in WT, Δ*kinA*, and Δ*sda* strains.

Figure S5: *tapA* expression is not in a steady-state during simulation. The red and black line shows the dynamics of mean TapA levels of WT and Δ*kinC* strains, which are the same as Fig. 4B. The green line shows the mean TapA levels of Δ*kinC* strain for simulations assuming the growth rate stops decreasing at T6 and is fixed thereafter.

Figure S6: Stochastic simulation of the model.
(A) The algorithm of the stochastic simulation for the starving condition.
(B) The correction of the growth rate is used in the stochastic simulation. The red line shows the growth rate given by the deterministic model, the same as Fig. 2A. The dashed line shows the population growth rate reproduced by the stochastic model without correction. The blue line shows the population growth rate reproduced by the stochastic model with $k = 0.2$.
Table S1: Parameters of the model for the growth dynamics

Table S2: Reactions and parameters of the stochastic model of SinI-SinR-SlrR network.

Table S3: List of strains and plasmids used in this work

Text S1: Supplemental Computational Methods

Acknowledgment

We are very grateful to Yunrong Chai for useful discussions and comments on an earlier draft of the manuscript. We also thank the Bacillus Genetic Stock Center (Ohio State University) for providing bacterial strains and plasmids. The work is supported by the National Science Foundation (MCB-1616755 to OAI and MCB-1616761 to MF), and the Welch Foundation (Grant C-1995 to OAI).

References

1. Storz G, Hengge R. 2011. Bacterial Stress Responses, Second Edition. American Society of Microbiology.
2. Branda SS, Gonzalez-Pastor JE, Ben-Yehuda S, Losick R, Kolter R. 2001. Fruiting body formation by Bacillus subtilis. Proceedings of the National Academy of Sciences of the United States of America 98:11621-11626.
3. Kearns DB, Chu F, Branda SS, Kolter R, Losick R. 2005. A master regulator for biofilm formation by Bacillus subtilis. Molecular Microbiology 55:739-749.
4. Flemming H-C, Wingender J, Szewzyk U, Steinberg P, Rice SA, Kjelleberg S. 2016. Biofilms: An emergent form of bacterial life. Nature Reviews Microbiology 14:563-575.
5. Riley EP, Schwarz C, Derman AI, Lopez-Garrido J. 2020. Milestones in Bacillus subtilis sporulation research. Microbial Cell 8:1-16.
6. van Gestel J, Vlamakis H, Kolter R. 2015. From Cell Differentiation to Cell Collectives: Bacillus subtilis Uses Division of Labor to Migrate. PLOS Biology 13:e1002141.
7. Vlamakis H, Chai Y, Beauregard P, Losick R, Kolter R. 2013. Sticking together: Building a biofilm the Bacillus subtilis way. Nature Reviews Microbiology 11:157-168.
8. Burbulys D, Trach KA, Hoch JA. 1991. Initiation of sporulation in B. Subtilis is controlled by a multicomponent phosphorelay. Cell 64:545-552.
9. Jiang M, Shao W, Perego M, Hoch JA. 2000. Multiple histidine kinases regulate entry into stationary phase and sporulation in Bacillus subtilis. Molecular Microbiology 38:535-542.
10. Fujita M, Losick R. 2005. Evidence that entry into sporulation in Bacillus subtilis is governed by a gradual increase in the level and activity of the master regulator Spo0A. Genes & development 19:2236-2244.
11. Chen Z, Srivastava P, Zarazúa-Osorio B, Marathe A, Fujita M, Igoshin OA. 2022. Bacillus subtilis histidine kinase KinC activates biofilm formation by controlling heterogeneity of single-cell responses. Mbio 13:e01694-21.
12. Devi SN, Vishnoi M, Kiehler B, Haggett L, Fujita M. 2015. In vivo functional characterization of the transmembrane histidine kinase KinC in Bacillus subtilis. Microbiology 161:1092-1104.
13. Molle V, Fujita M, Jensen ST, Eichenberger P, González-Pastor JE, Liu JS, Losick R. 2003. The Spo0A regulon of Bacillus subtilis. Molecular Microbiology 50:1683-1701.
14. Narula J, Kuchina A, Lee D-YD, Fujita M, Süel GM, Igoshin OA. 2015. Chromosomal Arrangement of Phosphorelay Genes Couples Sporulation and DNA Replication. Cell 162:328-337.
15. Narula J, Kuchina A, Zhang F, Fujita M, Süel GM, Igoshin OA. 2016. Slowdown of growth controls cellular differentiation. Molecular Systems Biology 12:871.
16. Narula J, Devi SN, Fujita M, Igoshin OA. 2012. Ultrasensitivity of the Bacillus subtilis sporulation decision. Proceedings of the National Academy of Sciences 109:E3513-E3522.
17. Bai U, Mandic-Mulec I, Smith I. 1993. SinI modulates the activity of SinR, a developmental switch protein of Bacillus subtilis, by protein-protein interaction. Genes & Development 7:139-148.
18. Chai Y, Chu F, Kolter R, Losick R. 2008. Bistability and biofilm formation in Bacillus subtilis. Molecular microbiology 67:254-263.
19. Shafikhani SH, Mandic-Mulec I, Strauch MA, Smith I, Leighton T. 2002. Postexponential regulation of sin operon expression in Bacillus subtilis. Journal of Bacteriology 184:564-571.
20. DeLoughery A, Dengler V, Chai Y, Losick R. 2016. Biofilm formation by Bacillus subtilis requires an endoribonuclease-containing multisubunit complex that controls mRNA levels for the matrix gene repressor SinR. Mol Microbiol 99:425-37.

21. Colledge VL, Fogg MJ, Levdikov VM, Leech A, Dodson EJ, Wilkinson AJ. 2011. Structure and Organisation of SinR, the Master Regulator of Biofilm Formation in Bacillus subtilis. Journal of Molecular Biology 411:597-613.
22. Milton ME, Draughn GL, Bobay BG, Stowe SD, Olson AL, Feldmann EA, Thompson RJ, Myers KH, Santoro MT, Kearns DB, Cavanagh J. 2020. The Solution Structures and Interaction of SinR and SinI: Elucidating the Mechanism of Action of the Master Regulator Switch for Biofilm Formation in Bacillus subtilis. Journal of Molecular Biology 432:343-357.
23. Newman JA, Rodrigues C, Lewis RJ. 2013. Molecular basis of the activity of SinR protein, the master regulator of biofilm formation in Bacillus subtilis. The Journal of Biological Chemistry 288:10766-10778.
24. Chai Y, Norman T, Kolter R, Losick R. 2011. Evidence that metabolism and chromosome copy number control mutually exclusive cell fates in Bacillus subtilis. The EMBO Journal 30:1402-1413.
25. Norman TM, Lord ND, Paulsson J, Losick R. 2013. Memory and Modularity in Cell-Fate Decision Making. Nature 503:481-486.
26. Chu F, Kearns DB, Branda SS, Kolter R, Losick R. 2006. Targets of the master regulator of biofilm formation in Bacillus subtilis. Molecular Microbiology 59:1216-1228.
27. Fujita M, González-Pastor JE, Losick R. 2005. High- and Low-Threshold Genes in the Spo0A Regulon of Bacillus subtilis. Journal of Bacteriology 187:1357-1368.
28. Eswaramoorthy P, Dinh J, Duan D, Igoshin OA, Fujita M. 2010. Single-cell measurement of the levels and distributions of the phosphorelay components in a population of sporulating Bacillus subtilis cells. Microbiology (Reading, England) 156:2294-2304.
29. López D, Kolter R. 2010. Extracellular signals that define distinct and coexisting cell fates in Bacillus subtilis. FEMS microbiology reviews 34:134-149.
30. Lord ND, Norman TM, Yuan R, Bakshi S, Losick R, Paulsson J. 2019. Stochastic antagonism between two proteins governs a bacterial cell fate switch. Science (New York, NY) 366:116-120.
31. Ogura M. 2016. Post-transcriptionally generated cell heterogeneity regulates biofilm formation in Bacillus subtilis. Genes to Cells 21:335-349.
32. Narula J, Fujita M, Igoshin OA. 2016. Functional requirements of cellular differentiation: Lessons from Bacillus subtilis. Current Opinion in Microbiology 34:38-46.
33. Eswaramoorthy P, Duan D, Dinh J, Dravis A, Devi SN, Fujita M. 2010. The Threshold Level of the Sensor Histidine Kinase KinA Governs Entry into Sporulation in Bacillus subtilis. Journal of Bacteriology 192:3870-3882.
34. Kovárová-Kovar K, Egli T. 1998. Growth Kinetics of Suspended Microbial Cells: From Single-Substrate-Controlled Growth to Mixed-Substrate Kinetics. Microbiology and Molecular Biology Reviews 62:646-666.
35. Chai Y, Kolter R, Losick R. 2010. Reversal of an Epigenetic Switch Governing Cell Chaining in Bacillus subtilis by Protein Instability. Molecular microbiology 78:218-229.
36. Slager J, Veening JW. 2016. Hard-Wired Control of Bacterial Processes by Chromosomal Gene Location. Trends Microbiol 24:788-800.
37. Kaplan S, Bren A, Dekel E, Alon U. 2008. The incoherent feed-forward loop can generate non-monotonic input functions for genes. Mol Syst Biol 4:203.
38. Ascensao JA, Datta P, Hancioglu B, Sontag E, Gennaro ML, Igoshin OA. 2016. Non-monotonic Response to Monotonic Stimulus: Regulation of Glyoxylate Shunt Gene-Expression Dynamics in Mycobacterium tuberculosis. PLoS Comput Biol 12:e1004741.
39. Rowland SL, Burkholder WF, Cunningham KA, Maciejewski MW, Grossman AD, King GF. 2004. Structure and Mechanism of Action of Sda, an Inhibitor of the Histidine Kinases that Regulate Initiation of Sporulation in Bacillus subtilis. Molecular Cell 13:689-701.

40. Ruvolo MV, Mach KE, Burkholder WF. 2006. Proteolysis of the replication checkpoint protein Sda is necessary for the efficient initiation of sporulation after transient replication stress in Bacillus subtilis. Molecular Microbiology 60:1490-1508.
41. Pan Q, Losick R. 2003. Unique degradation signal for ClpCP in Bacillus subtilis. J Bacteriol 185:5275-8.
42. Londoño-Vallejo JA, Frehel C, Stragier P. 1997. SpoIIQ, a forespore-expressed gene required for engulfment in Bacillus subtilis. Molecular microbiology 24:29-39.
43. Chai Y, Norman T, Kolter R, Losick R. 2010. An epigenetic switch governing daughter cell separation in Bacillus subtilis. Genes & Development 24:754-765.
44. Jaruszewicz-Błońska J, Lipniacki T. 2017. Genetic toggle switch controlled by bacterial growth rate. BMC Systems Biology 11:117.
45. Klumpp S, Hwa T. 2014. Bacterial growth: Global effects on gene expression, growth feedback and proteome partition. Current Opinion in Biotechnology 28:96-102.
46. Klumpp S, Zhang Z, Hwa T. 2009. Growth rate-dependent global effects on gene expression in bacteria. Cell 139:1366-1375.
47. Santiago E, Moreno DF, Acar M. 2021. Modeling aging and its impact on cellular function and organismal behavior. Experimental Gerontology:111577.
48. Konkol MA, Blair KM, Kearns DB. 2013. Plasmid-Encoded ComI Inhibits Competence in the Ancestral 3610 Strain of Bacillus subtilis. Journal of Bacteriology 195:4085-4093.
49. Nye TM, Schroeder JW, Kearns DB, Simmons LA. 2017. Complete Genome Sequence of Undomesticated Bacillus subtilis Strain NCIB 3610. Genome Announc 5.
50. Harwood CRCSM. 1990. Molecular biological methods for Bacillus. Wiley, Chichester; New York.
51. Sambrook JRDW. 2001. Molecular cloning : a laboratory manual. Cold Spring Harbor Laboratory Press, Cold Spring Harbor, N.Y.
52. Guérout-Fleury AM, Frandsen N, Stragier P. 1996. Plasmids for ectopic integration in Bacillus subtilis. Gene 180:57-61.
53. Wang X, Montero Llopis P, Rudner DZ. 2014. Bacillus subtilis chromosome organization oscillates between two distinct patterns. Proc Natl Acad Sci U S A 111:12877-82.

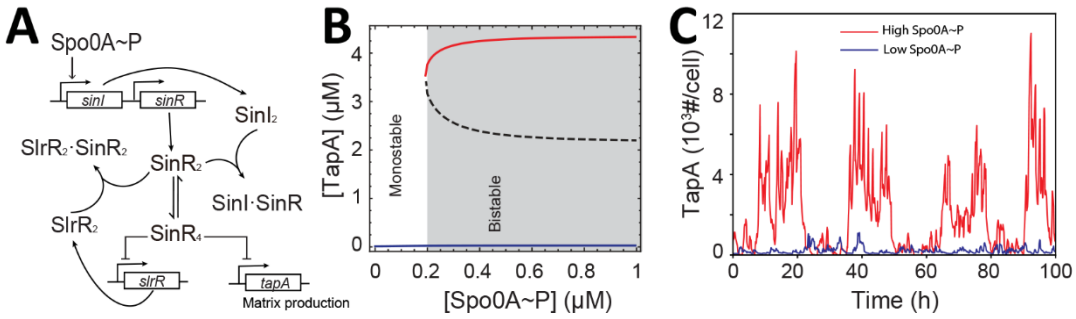

Figure 1: Bistable expression of *tapA* is controlled by the Spo0A~P level via the SinI-SinR-SlrR network. (A) The schematic of the SinI-SinR-SlrR network used in our model (see SI: Methods for details). **(B)** Deterministic model of the network predicts the existence of two steady states high (red) and low (blue) TapA steady-state concentration. At low Spo0A~P concentrations (< 0.2 μM), only a low steady state exists (monostability). At high Spo0A~P concentrations (> 0.2 μM), two stable steady states co-exist in the bistable region (shaded area). Unstable steady state separating the two is show by dashed line. **(C)** Stochastic simulation of *tapA* expression as a function of time was performed using the fixed Spo0A~P concentrations at low (0.05 μM, blue line, value from the monostable region in (B)) or at high (1 μM red line, value from the bistable region in (B)). The x- and y-axis indicate time (h) and *tapA* TapA levels in number of molecule per cell(#/cell), respectively.

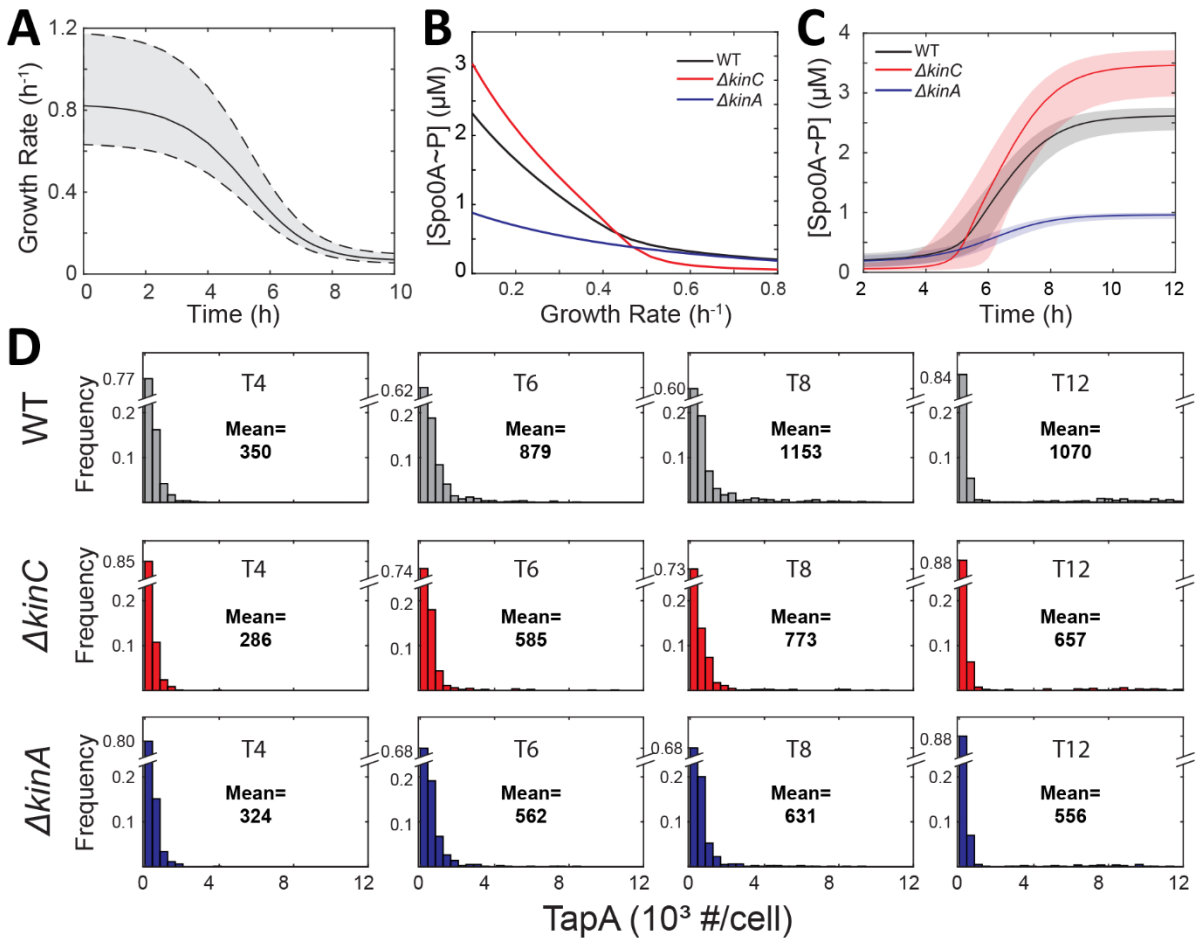

Figure 2: Heterogeneity of *tapA* expression is controlled by growth rate and the SinI-SinR-SlrR network. (A)The dynamics and fluctuation (shaded area shows ±σ region) of growth rate (y-axis) over time (x-axis) predicted by a Moser-type model (34). **(B)** Model-predicted Spo0A~P concertation (y-axis) as a function of the growth rate (x-axis) in the WT, Δ*kinC*, and Δ*kinA* strains. **(C)** Predicted Spo0A~P dynamics and fluctuations as a function of time (shaded area shows ±σ region) in the WT, Δ*kinC*, and Δ*kinA* strains. **(D)** Prediction of single-cell distribution of *tapA* expression at T4, T6, T8, and T12 in the WT, Δ*kinC*, and Δ*kinA* strains using the results of (C) as an input to stochastic model of the SinI-SinR-SlrR network. Population mean levels of *tapA* expression (number of TapA molecules/cell) are indicated in each panel. Note that the maximum value for the first bin is indicated in the broken y-axis with the same scale for the remaining bins used in each panel.

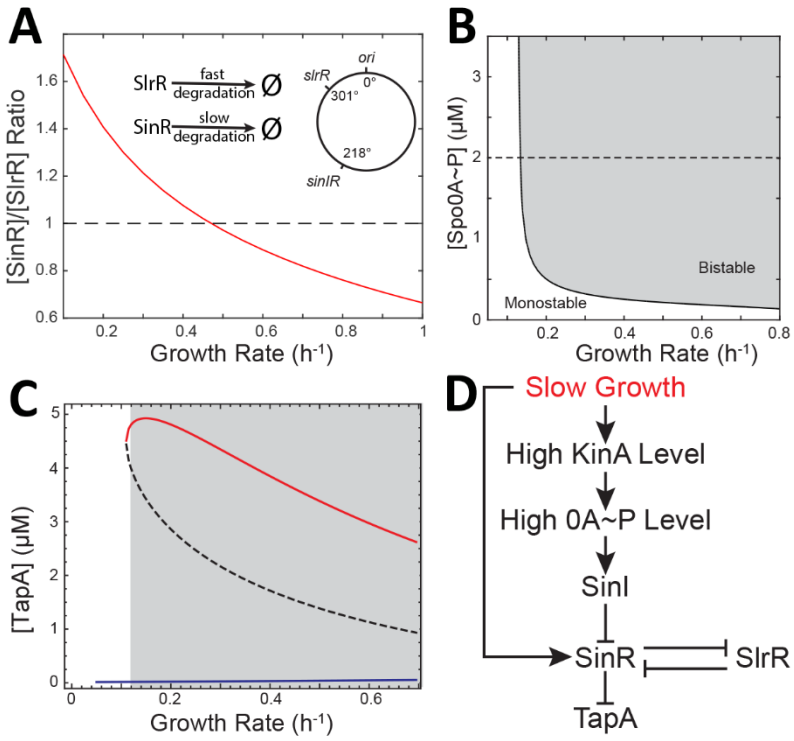

Figure 3: The behavior of the SinI-SinR-SlrR network is determined by both the Spo0A~P level and the growth rate. (A) Changes in the predicted ratio of the relative concentrations between SinR and SlrR as a function of growth rate. The inset illustrates degradation rates of SlrR and SinR, and their gene positions on the chromosome. **(B)** Bifurcation between mono- (clear) and bi-stability (shaded) of *tapA* expression state controlled by Spo0A~P level (y-axis) and growth rate (x-axis) via SinI-SinR-SlrR network. **(C)** High (red) and low (blue) steady states of TapA concentration as a function of growth rate at the fixed 2μM Spo0A~P condition as indicated with the dashed line in panel B. The shaded region shows a bistable region in which high TapA-expressing state is possible (red). Decrease of the growth rate outside of the bistable region lead to switch into deactivated *tapA* expression state (blue line). **(D)** The proposed feed-forward network showing how growth rate regulates biofilm matrix production via the SinI-SinR-SlrR network.

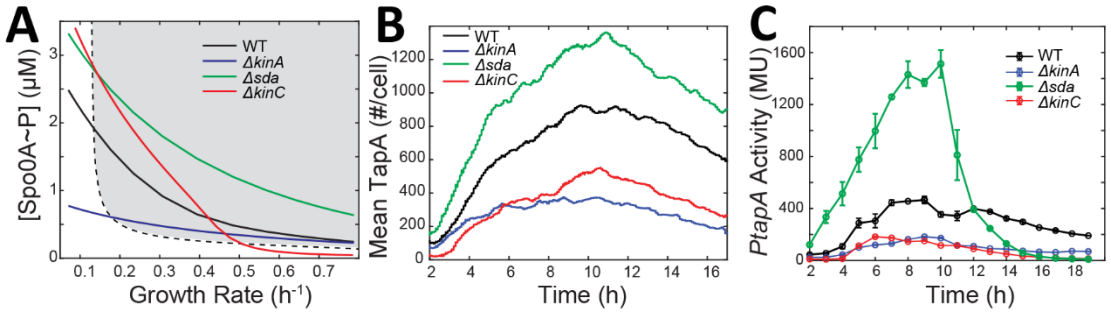

Figure 4: Repression of *tapA* expression caused by slowdown of growth rate. (A) Predicted changes in Spo0A~P concentration as a function of growth rate in the WT, Δ*kinA*, Δ*kinC*, and Δ*sda* strains superimposed on the Fig. 3B displaying bifurcation (dashed line) between mono- (clear) and bi-stability (shaded) of *tapA* expression state controlled via the SinI-SinR-SlrR network. **(B)** Stochastic simulation of *tapA* expression dynamics in the WT, Δ*kinA*, Δ*kinC*, and Δ*sda* strains. The x- and y-axis indicate time (h) and population-averaged (mean of N=1000 simulations) *tapA* expression levels (number of molecules/cell), respectively. **(C)** Experimentally measured *tapA* expression at a population level in the WT, Δ*kinA*, Δ*kinC*, and Δ*sda* strains. Culture samples were collected at the indicated times (x-axis) after the start of incubation and assayed for β-Galactosidase activity from *PtapA-lacZ* (Miller units, MU, y-axis). The mean activities of three independent experiments are shown with standard deviations as error bars.

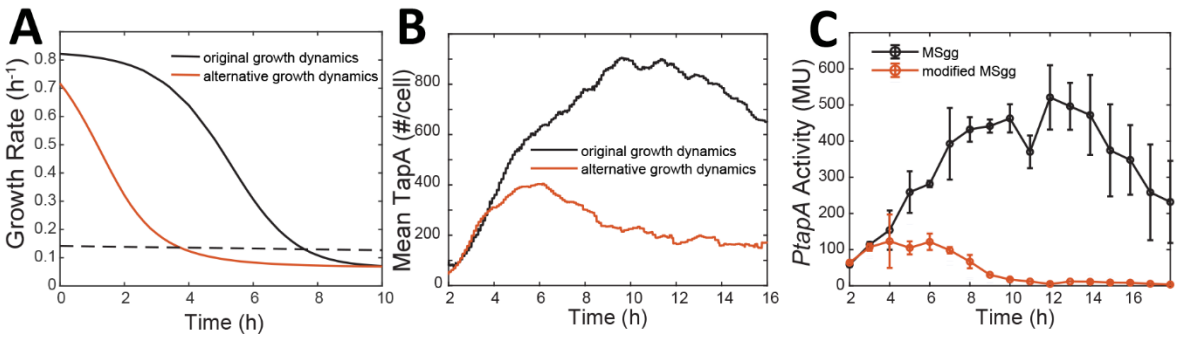

Figure 5: The dynamics of *tapA* expression under different growth dynamics. (A) Stochastic simulation of growth rate (y-axis) as a function of time (x-axis) under normal (black) and slow (red) growth conditions.

When different growth dynamics depicted in **(A)** were used as an input in our stochastic simulations, the model predicted **(B)** Stochastic simulation of *tapA* expression (mean number of TapA molecule per cell, y-axis) as a function of time (x-axis) under normal (black) and slow (red) growth conditions.

(C) Experimentally measured *tapA* expression at a population level in the WT cells grown in normal (black) and nitrogen-reduced (reduced to one tenth of the normal level, red) MSgg medium. Culture samples were collected at the indicated times (x-axis) after the start of incubation and assayed for β-galactosidase activity from *PtapA-lacZ* (Miller units, MU, y-axis). The mean activities of three independent experiments are shown with standard deviations.

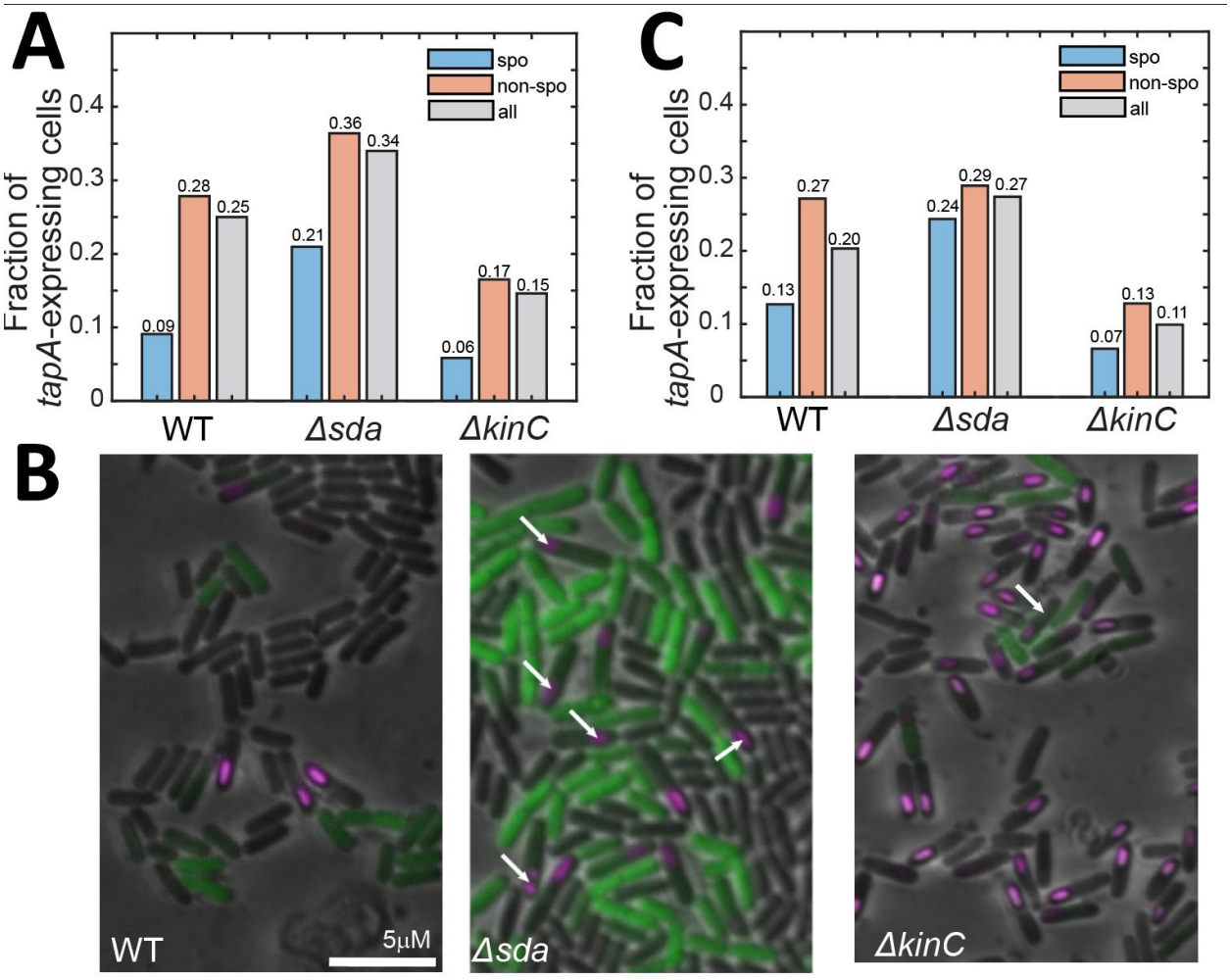

Figure 6: Acceleration of Spo0A~P dynamics decrease mutual exclusiveness of sporulation and matrix production (A) Stochastic simulation of *tapA* expression in sporulating (spo, slow growth), nonsporulating (non-spo, fast growth), and all cells in the WT, Δ*sda*, and Δ*kinC* strains. **(B)** Fluorescent images of the WT, Δ*sda*, and Δ*kinC* cells harboring both GFP-LCN (unstable GFP) reporter under the control of *tapA* promoter (*PtapA-gfp-lcn*) and mCherry reporter under the control of *spoIIQ* promoter (*PspoIIQ-mCherry*). Cells were cultured in MSgg medium and processed for imaging at 8 h after the start of culture. Cells displaying both GFP (*tapA* expression) and mCherry (*spoIIQ* expression for sporulation) are indicated with arrows. Scale bar: 5 μm. (C) The experimentally measured fraction of cells expressing *tapA* in sporulating (spo) cells, non-sporulating (non-spo) cells, and all cells in WT, Δ*sda*, and Δ*kinC* strains.